Parameterizing Subgrid Orographic Precipitation and Surface Cover in Climate Models

L. R. LEUNG AND S. J. GHAN

Pacific Northwest National Laboratory, Richland, Washington

ABSTRACT

Previous development of the Pacific Northwest National Laboratory's regional climate model has focused on representing orographic precipitation using a subgrid parameterization where subgrid variations of surface elevation are aggregated to a limited number of elevation classes. An airflow model and a thermodynamic model are used to parameterize the orographic uplift/descent as air parcels cross over mountain barriers or valleys. This paper describes further testing and evaluation of this subgrid parameterization. Building upon this modeling framework, a subgrid vegetation scheme has been developed based on statistical relationships between surface elevation and vegetation. By analyzing high-resolution elevation and vegetation data, a dominant land cover is defined for each elevation band of each model grid cell to account for the subgrid heterogeneity in vegetation. When larger lakes are present, they are distinguished from land within elevation bands and a lake model is used to simulate the thermodynamic properties. The use of the high-resolution vegetation data and the subgrid vegetation scheme has resulted in an improvement in the model's representation of surface cover over the western United States. Simulation using the new vegetation scheme yields a 1°C cooling when compared with a simulation where vegetation was derived from a 30-min global vegetation dataset without subgrid vegetation treatment; this cooling helps to reduce the warm bias previously found in the regional climate model. A 3-yr simulation with the subgrid parameterization in the climate model is compared with observations.

1. Introduction

Topography is a prominent feature in many regions of the world. High spatial resolution is required to accurately simulate precipitation and surface hydrology associated with heterogeneity in surface elevation and vegetation in those areas. This is feasible when one is interested in case studies of atmospheric processes, but it is computationally very demanding for climate simulations. It is not surprising that many scientific research programs, such as the Global Energy and Water Cycle Experiment (GEWEX) (International GEWEX Project Office 1994; Shuttleworth 1996), have emphasized the importance of representing subgrid-scale variability in precipitation, and its effects on model-simulated hydrologic cycle.

Recently, Leung and Ghan (1995) introduced a subgrid orographic precipitation parameterization that addresses this issue. The parameterization yields separate predictions of precipitation, temperature, snow water equivalent, soil moisture, and surface runoff for a selected number of surface elevation classes within each grid cell. For each surface elevation class, cloud processes are treated using a bulk microphysics parameterization, and land surface processes are modeled using a one-dimensional surface physics scheme. The simulated fields can be distributed according to the spatial distribution of surface elevation within each grid cell to yield predictions at the scale of the surface elevation data.

This subgrid parameterization has been implemented in the Pacific Northwest National Laboratory's Regional Climate Model (PNNL-RCM). Leung and Ghan (1995) summarized different aspects of resulting improvements in precipitation and snow cover simulation in the Pacific Northwest. They evaluated the precipitation simulation at both daily and monthly timescales and over different spatial scales. Leung and Ghan (1995) concluded that a simulation performed at 90-km grid resolution with the subgrid parameterization is superior to simulations performed at 90-km or 30-km grid resolutions but without the subgrid parameterization. Furthermore, the atmospheric simulation has been used to drive a detailed surface hydrology model at the Middle Fork Flathead watershed in Montana to evaluate the usefulness of the subgrid parameterization in providing detailed atmospheric forcings for simulating streamflow, soil moisture, and snow cover in remote mountainous areas (Leung et al. 1996). The simulation of streamflow and snow cover was found to compare favorably with observations when the hydrology model was driven by the

Corresponding author address: Dr. L. R. Leung, Pacific Northwest National Laboratory, P.O. Box 999/MS K9-30, Richland, WA 99352. E-mail: ruby.leung@pnl.gov

climate simulation generated with the use of the subgrid orographic precipitation scheme. The first part of this paper describes further evaluation and analysis of the subgrid parameterization of orographic precipitation using sensitivity experiments and a longer simulation. To complement previous work by Leung and Ghan (1995), the sensitivity experiments focus more on evaluation at the local scale; that is, precipitation simulated for a range of surface elevation within specific grid cells.

We continue to build upon the existing modeling framework to account for subgrid variations in vegetation cover. Several subgrid representations of surface cover exist in the literature; they can be grouped into two categories. The first kind of subgrid representation (e.g., Avissar 1992; Entekhabi and Eagleson 1989) determines the probability distribution of subgrid vegetation within model grid cells and accounts for the subgrid effects through stochastic-dynamical models of surface processes. The second kind of subgrid representation is called the ''mosaic'' approach where each model grid cell is subdivided into an arbitrary number of vegetation types; surface processes are modeled over each vegetation type and are then coupled independently to the model grid-cell-mean atmospheric column. Examples of this method include Koster and Suarez (1992), Raupach (1993), among others.

More recently, several studies (e.g., Pielke et al. 1991; Avissar and Chen 1993) have suggested that surface heterogeneity not only affects the atmospheric column directly above the surface, but through secondary circulations forced by differential heating over contrasting land cover on adjacent patches, it affects the structure and dynamics of the boundary layer over the whole area. An attempt to model this secondary effect has been made by Zeng and Pielke (1994), who parameterized secondary circulations as mesoscale turbulence processes. Based on case studies over the Southern Great Plains, Zhong and Doran (1995, 1997), however, questioned the importance of representing mesoscale fluxes associated with secondary circulations under more realistic conditions of surface heterogeneity.

Our approach is similar to the mosaic representation in that each elevation class is further divided into multiple land cover types. In principle, one can specify the accuracy needed in the subgrid vegetation representation and determine the number of surface classes for each model grid cell. We will describe a statistical analysis of high spatial resolution surface elevation and vegetation data to represent subgrid variations in surface cover. The new subgrid vegetation scheme will be tested over the Pacific Northwest through sensitivity experiments. We also describe the implementation of a lake model, as subgrid lakes can now be captured by the subgrid surface scheme. A 3-yr simulation is then performed with the subgrid parameterization of orographic precipitation and surface cover, and the lake model over the Pacific Northwest. The simulation is evaluated by comparing the results with observations.

2. Model description

The regional climate model is based on the hydrostatic version of the Penn State/National Center for Atmospheric Research (NCAR) Mesoscale Model (MM5) (Anthes et al. 1987; Grell et al. 1993). Several physical parameterizations important on climatic timescales have been applied to the model for climate applications. These parameterizations include a two-stream delta-Eddington treatment for shortwave radiation (Taylor and Ghan 1992) and an emissivity approach for longwave radiation (Kiehl et al. 1987), a bulk cloud microphysics scheme that distinguishes liquid and ice phase (Cotton et al. 1986; Ghan and Easter 1992), and a surface physics scheme (BATS) (Dickinson et al. 1993). Grell's parameterization scheme (Grell 1993) is used to treat cumulus convection. For the planetary boundary layer the high-resolution model of Zhang and Anthes (1982) is used.

The most noteworthy feature of the regional climate model is the introduction of a parameterization of subgrid-scale orographic processes (Leung and Ghan 1995). The parameterization is based on an elevation model that aggregates subgrid variations of surface elevation to a limited number of elevation bands. A simple airflow model and a thermodynamic model are used to account for orographic uplifting of an airmass as it crosses over subgrid hills or valleys. Physical processes such as cloud and precipitation, radiation, boundary layer turbulence, and surface physics are all calculated for each elevation band of each grid cell.

In the past, the RCM defined one vegetation type for each grid cell, even though vegetation can vary strongly within grid cells of 90 km or more. To improve the representation of vegetation and hence the simulation of surface processes, a subgrid vegetation scheme has been developed based on the surface elevation dependence of vegetation. Taking advantage of the elevation classification already implemented in the climate model, the general framework for the vegetation scheme is such that one can further divide each elevation band into a number of surface cover types. Lakes that are normally too small to be represented by climate model grid cells can now be included in the model. A thermodynamic lake model is used to simulate lake temperature and ice. We will describe each parameterization in more detail in the following.

a. Elevation model

The surface elevation model is based on the statistical subgrid approach of Avissar and Pielke (1989) and Avissar (1992). Subgrid variations in surface elevation are aggregated into a modest number of surface elevation classes. The surface elevation model carries no information about the spatial distribution of each surface class other than the fractional area and mean elevation of each class within each grid cell. A 30 arc s surface

TABLE 1. Classification of surface elevation.

Class	Elevation, m
1	0–100
2	100–200
3	200–300
4	300–400
5	400–500
6	500–700
7	700–1000
8	1000–1500
9	1500–2000
10	2000–3000
11	3000–4000
12	4000–5000

elevation dataset (Guo and Chen 1993) is used to determine the fractional area and mean elevation of each class, with the classes defined by a predetermined set of surface elevation ranges (Table 1). Some grid cells may have as many as 12 elevation classes, whereas others may only have one. Separate calculations of atmospheric and surface processes are performed for each surface class, with feedback to the grid scale accomplished by forming an area-weighted average of processes and variables within each grid cell.

b. Subgrid orographic precipitation scheme

A simple airflow model (Leung and Ghan 1995) is used to determine the subgrid height rise or descent of air parcels flowing through barrier/valley. The nondimensional mountain height (or Froude number) is used to determine the flow regime,

$$\text{Fr} = NH/U, \tag{1}$$

where U is the wind speed, N is the Brunt-Väisälä frequency, and H is the height of the mountain defined here as $z_n - \overline{z}_s$, where z_n is the height of surface elevation class n and $\overline{z}_s$ is the height of the grid cell mean surface elevation. The height rise of air parcels is given by

$$h_n = \min(H, \text{Fr}_c U/N), \tag{2}$$

where Fr_c is a critical Froude number of order one. When Fr is smaller than Fr_c, all flow goes over the mountain [$h_n = H$ follows from (2)]. At larger Fr (Fr $>$ Fr_c), part of the low-level flow becomes blocked and goes around mountain (e.g., Sheppard 1956; Smith 1980, 1989; Lott and Miller 1997). The depth of the blocking layer is given by

$$z_b = H - \text{Fr}_c(U/N). \tag{3}$$

Below z_b, air parcels at an altitude z will experience a height rise given by

$$h_n = \text{Fr}_c(U/N)(z/z_b), \tag{4}$$

while above z_b, (2) still applies.

The thermodynamic model determines the immediate impact of the subgrid height rise/descent on temperature

and humidity. The thermodynamic and cloud variables θ_c and r_w are used in this procedure because of their conservative properties during condensation as well as advection. They are defined as (Betts 1973)

$$\theta_c = \theta - (L/c_p)(r_c/E), \tag{5}$$

$$r_w = r_v + r_c, \tag{6}$$

where θ is the potential temperature; E is the Exner function; and r_c and r_v are the mixing ratios of cloud water and water vapor, respectively. Since in the absence of precipitation the variables θ_c and r_w are conserved as an air parcel passes over a mountain barrier, their vertical distributions in subgrid surface elevation class n, X_n^*, can be diagnosed from the vertical distribution of the grid cell mean, $\overline{X}$,

$$X_n^*(z) = \overline{X}(z - h_n), \tag{7}$$

where h_n is the height rise/descent of the air parcel determined by (2) to (4), and z is any particular height. The value of $\overline{X}$ at height $z - h_n$ is obtained by interpolation from the vertical distribution $\overline{X}(z)$. This diagnostic procedure yields the vertical distributions of X for each surface elevation class. The vertical distributions of other cloud species, such as cloud ice mixing ratio r_i and ice number density N_i, are also determined for each elevation class from the grid cell mean in the same way.

For cloud microphysical calculations, the temperature T, cloud water r_c, and water vapor r_v can be diagnosed from θ_c, r_w, and the pressure p by assuming r_v never exceeds the water vapor saturation mixing ratio $r_s(T, p)$. Here the pressure p for each elevation class at a vertical level σ is estimated from $p = \sigma p_n$, where p_n is the surface pressure of elevation class n and $\sigma \equiv p/p_n$ is the terrain-following vertical coordinate of the model. The surface pressure for each elevation class can be inferred from the grid cell mean surface pressure $\overline{p}_s$ using the linearized hydrostatic relation

$$p_n = \overline{p}_s e^{-(z_n - \overline{z}_s)/\overline{H}}, \tag{8}$$

where $\overline{H}$ is the density-scale height. Therefore, elevation classes with higher surface elevations have lower surface pressures, which from the definition of θ_c yield colder temperatures and higher cloud water concentrations.

We have found that simply diagnosing the subgrid variables from (7) overestimates the orographic signature of precipitation because it implies instantaneous subgrid mixing. We have therefore introduced a prognostic treatment for each elevation class forced by an orographic tendency,

$$\frac{\partial X_n}{\partial t} = \text{ADV}_n + F_{H_n} + O_n + Q_n, \tag{9}$$

where X represents θ_c, r_w, or other cloud species, ADV is the horizontal and vertical advection, F_H is the horizontal diffusion, and Q_n is a source term. The oro-

graphic tendency O_n is parameterized in terms of the subgrid profiles,

$$O_n = \frac{X_n^* - X_n}{\tau}, \tag{10}$$

where X_n^* is the orographic profile diagnosed from the height rise and the grid cell mean profile according to (7) and τ is the timescale for lifting/descent. The source term Q_n, which includes radiative heating, cloud microphysics, cumulus convection, and vertical mixing, is calculated for each elevation class. The advection and horizontal diffusion terms are interpolated vertically from the grid cell mean terms.

The prognostic equations for the grid cell mean variables, $\overline{X}$, can be expressed as

$$\frac{\partial \overline{X}}{\partial t} = \text{ADV}(\overline{X}) + F_H(\overline{X}) + \overline{Q}. \tag{11}$$

The subgrid source terms Q_n are aggregated to form $\overline{Q}$.

The subgrid parameterization extends to the surface, which is forced by different atmospheric conditions (radiative fluxes, temperature, water vapor, precipitation) for each surface elevation class. Separate calculations of surface processes are performed for each surface elevation class. At the completion of the simulation, variables predicted for each elevation class can be mapped to different geographical locations according to the high-resolution distribution of surface elevation. This mapping yields high-resolution two-dimensional spatial distributions of surface temperature, precipitation, soil moisture, snow water equivalent, and runoff.

c. Subgrid vegetation scheme

To model subgrid land surface heterogeneity, we have introduced a simple dependence of subgrid surface type on subgrid elevation to take advantage of the modeling framework implemented for the subgrid orographic precipitation scheme. An extensive body of literature provides evidence in support of a relationship between surface elevation and vegetation type on scales less than 100 km (e.g., Whittaker 1956; Vankat 1982; Barbour et al. 1987). Based on the 30-s Advanced Very-High Resolution Radiometer (AVHRR) vegetation data for the continental United States (Loveland et al. 1991), a dataset has been developed for the Pacific Northwest that describes vegetation in terms of the BATS surface types at 1.5-km resolution. This dataset was used to develop statistical relationships between subgrid vegetation and surface elevation. Figure 1 shows the surface elevation and vegetation in the Pacific Northwest at 1.5-km resolution.

When subgrid elevation is classified according to Table 1, over the Pacific Northwest region there is a total of 78 grid cells within the regional climate model domain at 90-km resolution and a total of 451 surface elevation bands. On average, there are 4.96 vegetation types within each elevation band. There are 167 bands where the dominant vegetation type occupies more than 80% of the area within the band. If a single vegetation type (the dominant type) is used to define the vegetation within each grid cell (scheme A), 60% of the total area would be assigned a correct vegetation type. When one vegetation type (the dominant type) is used to define the vegetation within each elevation band of each grid cell (scheme B), 67% of the total area would be assigned a correct vegetation type.

If only the dominant vegetation type is used to describe the vegetation within each elevation band, the subgrid variability that could be accounted for is limited. To estimate this limit, we classified the surface elevation at every 100-m interval and repeated the above analysis (scheme C). Table 2 summarizes the percent area with correct vegetation type assigned when the different elevation classification schemes are used. Scheme C is similar to scheme B, except for the elevation classification. Although the use of more elevation classes explains more subgrid variability (73%) in the surface type, the improvement is modest, and the average number of surface elevation bands per grid cell quickly increases from 4.5 to 16.4 from scheme B to C. One reason for the small improvement in surface type characterization is that some subgrid variability in vegetation is simply not related to surface elevation. Furthermore, even within the Pacific Northwest region, with highly complex topography, only 9.7% of the total area is above 2000 m (where the intervals of surface elevation classification in the subgrid scheme is relatively wide). By dividing surface elevation at 100-m interval, the relationship between surface elevation and vegetation may be more refined, but the percent area with correct vegetation assigned increases only modestly.

Based on the above result, scheme B has been implemented in the PNNL-RCM. As a result, no extra computation is introduced by the subgrid vegetation scheme; the surface physics scheme is simply applied to a different surface cover over different elevation bands. Figure 2 shows the vegetation cover described by the subgrid vegetation scheme when mapped according to surface elevation at 1.5-km resolution. Also shown is the vegetation cover used in the model before the development of the subgrid vegetation scheme. The latter was derived from a 30-min global vegetation data provided by the MM5 modeling group at NCAR (Guo and Chen 1993). It is clear that the AVHRR data capture much more of the heterogeneity in surface cover, and the subgrid vegetation scheme further allows some subgrid spatial features to be represented in the model. The result is a more refined description of the surface cover in the western United States.

Figure 3 summarizes the percentage of vegetation cover for each elevation class from the AVHRR data and the subgrid vegetation scheme for the whole area where subgrid surface cover has been developed. The surface elevation classification follows that shown in
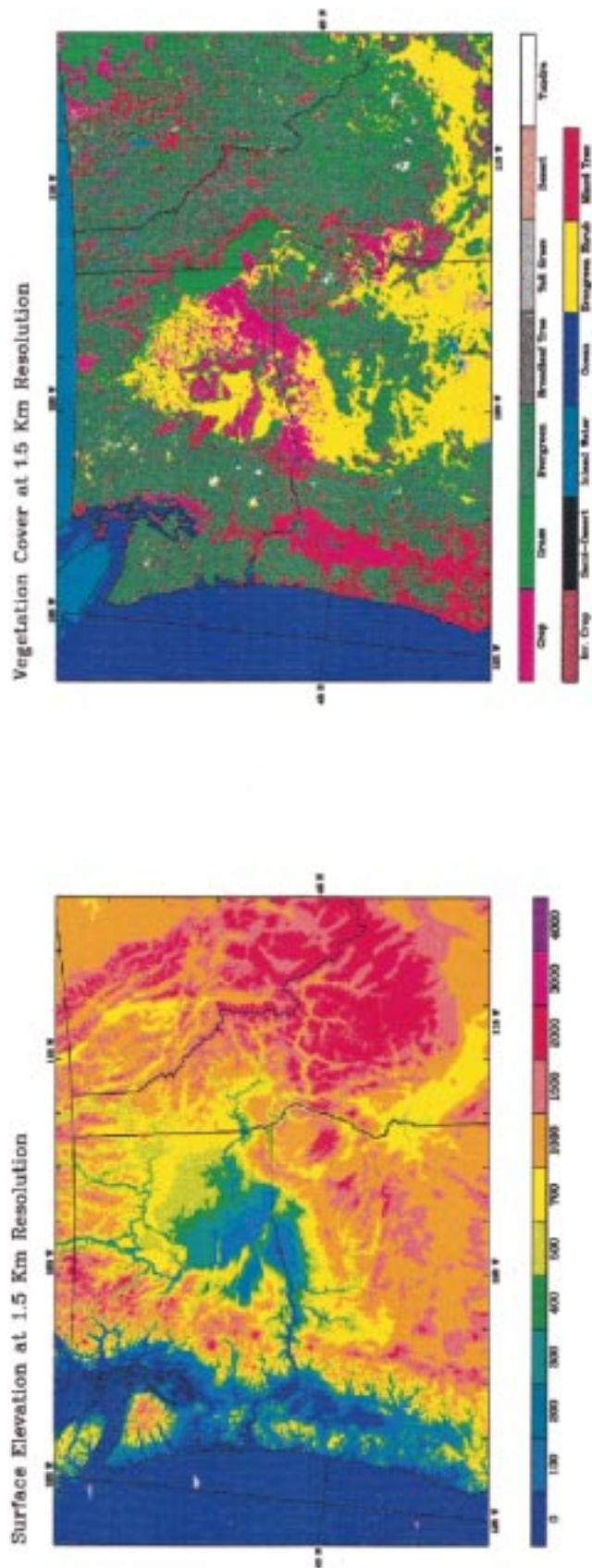
FIG. 1. Surface elevation and vegetation in the Pacific Northwest at 1.5-km spatial resolution. There are no vegetation data beyond the U.S.–Canada border.

TABLE 2. Statistics of vegetation-elevation analysis over the Pacific Northwest.

Vegetation scheme	% area with correct veg.	Avg. no. of elevation band
Scheme A	60.5	1
Scheme B	67.2	4.5
Scheme C	73.7	16.4

Table 1. Percentage surface cover is shown only for eight surface cover types; together they explain most of the variations in surface cover in the Pacific Northwest. At the lowest and highest elevation classes, surface cover is clearly dominated by a single cover type—ocean and tundra, respectively. In between the two extremes, there is a wide variety of vegetation cover. Generally, at the lower elevation (class 2 to class 6), there is a larger portion of crop, evergreen tree, and mixed tree. At the higher elevation, short grass, evergreen tree, evergreen shrub, and mixed tree are the major vegetation cover. Obviously, there is not a simple relationship between vegetation and surface elevation, as quite a variety of surface cover can be found within each elevation class. This is mainly because vegetation cover depends not only on surface elevation, but also on the environmental conditions supporting the vegetation. Areas belonging to the same elevation band, but under different climate conditions, will develop different vegetation cover. Therefore, it is very important that statistical relationships between vegetation and surface elevation be developed for each grid cell of the model domain. The distribution of vegetation for each elevation class as described by the subgrid representation generally follows that derived from observations. For each surface cover type, BATS is coupled directly with the atmospheric turbulence scheme to calculate the tendencies resulting from vertical mixing through the atmospheric column. These tendencies are applied to prognostic equations (9) for each elevation class, and are also aggregated to a grid cell mean according to the fractional vegetation cover; the grid cell mean tendency is applied to the prognostic equation (11). During postprocessing, simulations by BATS (e.g., surface temperature, soil moisture) for each surface cover type are mapped to geographical locations according to the high-resolution surface elevation dataset. If more than one surface type is prescribed within an elevation band, the high-resolution vegetation dataset is also used to perform the mapping.

d. Lake model

Adopting the subgrid surface cover representation (scheme B) described above, few inland water bodies can be included in the model because they seldom dominate a surface elevation class within a 90-km grid cell, unless the surface elevation class spans exceedingly fine elevation ranges. Because inland water is such an im-

portant source of water for the atmosphere, particularly in the arid western United States, we treat inland water as a separate surface type even if it is not the dominant surface type within an elevation band. However, we do not treat all inland water bodies as such because the small area of many inland water bodies does not justify the computational burden of including them. Only inland water bodies covering at least 2% of the area of a model grid cell are treated as a separate surface type.

Table 3 lists the inland water bodies identified by our selection criterion for the Pacific Northwest, including lake depth, turbidity, latitude and longitude of the nearest grid point, and the fractional area within its surface elevation class. Lake depth and turbidity have been estimated from an atlas, assuming relatively clear ($\eta = 0.1$ m^{-1}) water for deep lakes ($z > 20$ m) and relatively turbid ($\eta = 0.7$ m^{-1}) water for shallow lakes. The fractional area of lake water within elevation classes for 90-km grid cells ranges from 3%–54%. Figure 4 shows the locations of all the lakes in the Pacific Northwest at 1.5-km resolution. Also indicated are the locations and names of the 14 lakes represented by our subgrid surface cover scheme.

Following Hostetler et al. (1993) and Bates et al. (1995), lake surface temperature is predicted using the one-dimensional thermodynamic model of Hostetler and Bartlein (1990). This model replaces the BATS treatment of inland water, although surface evaporation and sensible heat flux are parameterized according to BATS rather than Hostetler and Bartlein (1990). The solar and longwave radiation at the lake surface are taken from the RCM treatment of radiative transfer, and the lake albedo is taken from BATS.

The treatment of lake ice is based on the bulk thermodynamic model of Patterson and Hamblin (1988). Heat diffusion at the surface has been corrected to read

$$q_0 = I_0 + \frac{K_i K_s}{h_s K_i + h_i K_s}(T_f - T_0) - \frac{K_i K_s}{h_s K_i + h_i K_s}I_0$$

$$\times \sum_n a_n \left[\frac{1 - \exp(-\lambda_{sn}h_s)}{K_s \lambda_{sn}} \right.$$

$$\left. + \exp(-\lambda_{sn}h_s)\frac{1 - \exp(-\lambda_{in}h_i)}{K_i \lambda_{in}} \right], \quad (12)$$

where I_0 is the net downward solar radiation at the surface; K_i and K_s are the thermal conductivities of ice and snow, respectively; h_i and h_s are the thickness of the ice and snow, respectively; T_f is the freezing temperature of water; T_0 is the surface temperature; a_n is the fraction of solar radiation in wavelength band n; and λ_{xn} is the absorption coefficient for wavelength band n for ice ($x = i$) and snow ($x = s$).

We have found that, because ice and particularly snow are such good insulators, the formation of ice and the accumulation of snow alter the lake energy balance considerably. As ice forms, heat loss from the water is only
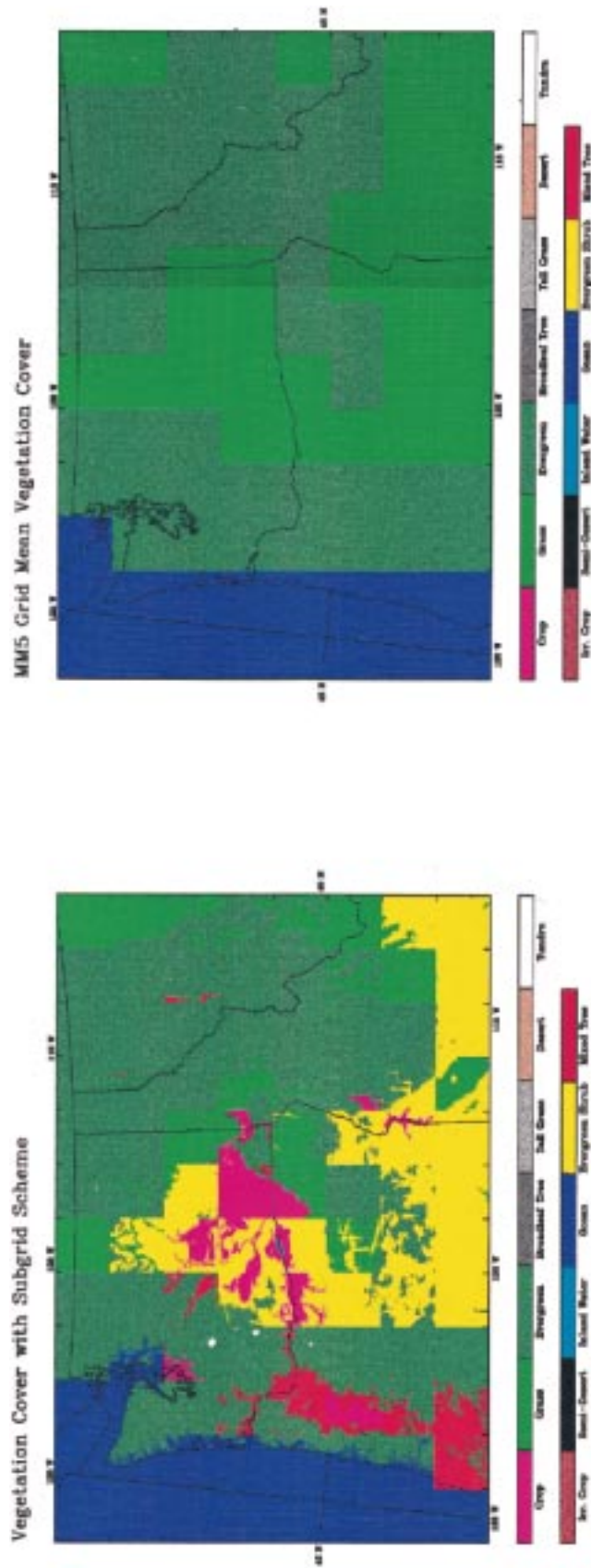
FIG. 2. Surface cover represented by (a) the subgrid surface cover scheme, and (b) 30-min global vegetation data, both mapped to 1.5-km resolution.
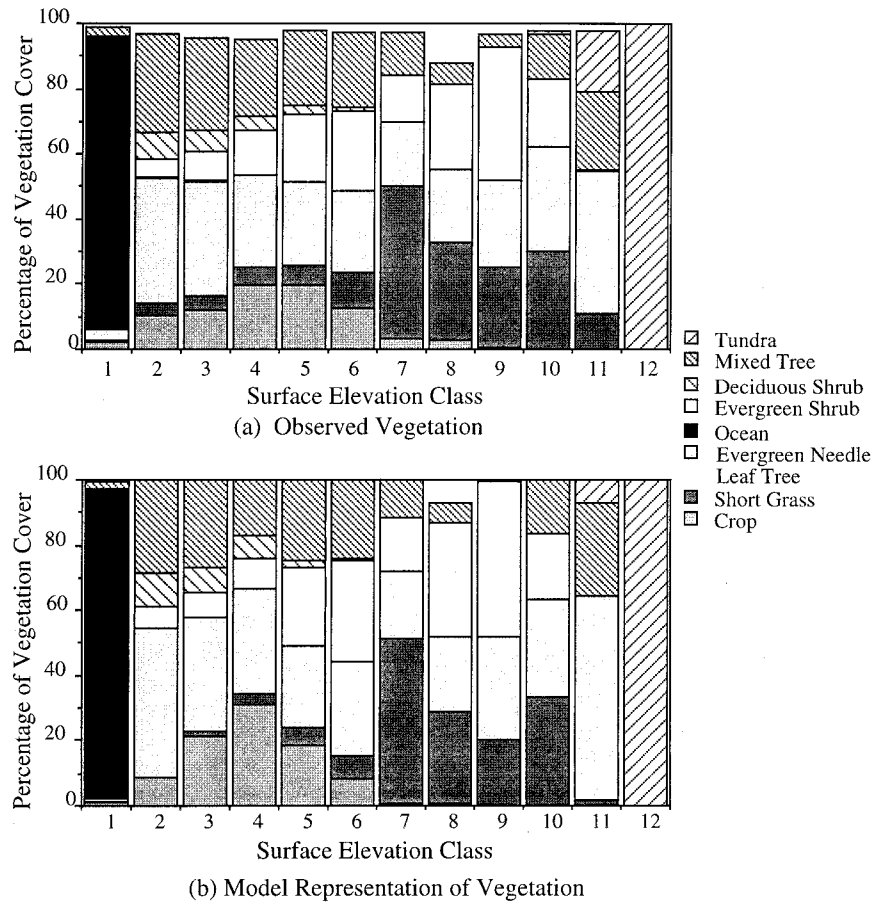
FIG. 3. Percentage of vegetation cover for each elevation class (see Table 1) summarized over all areas where the subgrid vegetation scheme has been applied. Statistics from AVHRR data are shown in (a) and that derived from the subgrid vegetation representation are shown in (b).

possible through exchange with the ice, which is much less efficient than the turbulent heat exchange between the surface and the atmosphere. Although absorption of solar radiation by the water is reduced by the high reflectivity of the ice and particularly the snow, and also by the absorption of solar radiation by the ice and snow,

enough solar radiation penetrates the ice and snow that warming of the water after ice formation can be noticeable. Some models avoid this problem by simply setting the water temperature equal to the melting temperature until the ice melts. However, this violates energy conservation and inhibits ice melt in the spring.

TABLE 3. Lake parameters used in the model.

| Lakes	Depth (m)	Turbidity	Latitude	Longitude	Fractional cover
Columbia River	10	0.7	46.3	123.1	0.13
Alkali Lakes	4	0.7	41.5	121.6	0.03
Klamath Lake	5	0.7	42.3	121.7	0.06
Goose Lake	4	0.7	41.6	120.6	0.09
Lake Albert	5	0.7	42.4	120.6	0.16
Pyramid Lake	100	0.1	40.0	119.5	0.09
Malheur Lake	2	0.7	43.2	118.5	0.05
Pend Oreille Lake	300	0.1	48.0	115.9	0.34
Flathead Lake	10	0.7	47.9	114.7	0.14
Salt Lake	14	0.7	40.6	113.3	0.07
Salt Lake	15	0.7	41.4	113.2	0.35
Utah Lake	15	0.7	40.5	112.3	0.28
Salt Lake	15	0.7	41.3	112.2	0.54
Yellowstone Lake	40	0.1	44.3	110.5	0.05

Locations of Subgrid Lakes
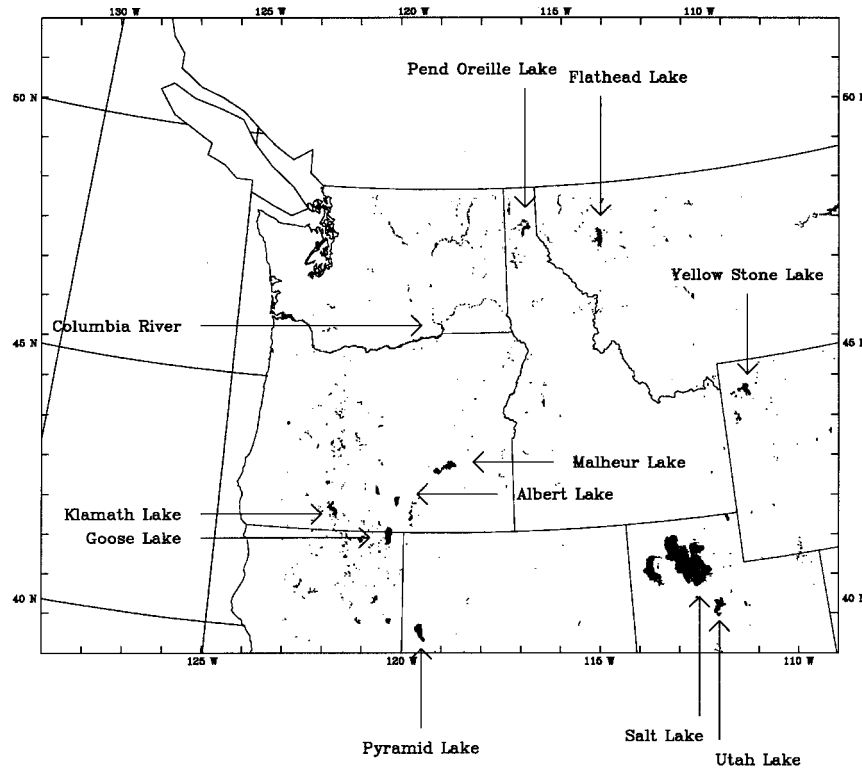
FIG. 4. The locations and sizes of lakes derived from the AVHRR data at 1.5-km resolution. Fourteen lakes or inland water bodies indicated by names are represented by the subgrid surface cover scheme in the climate model.
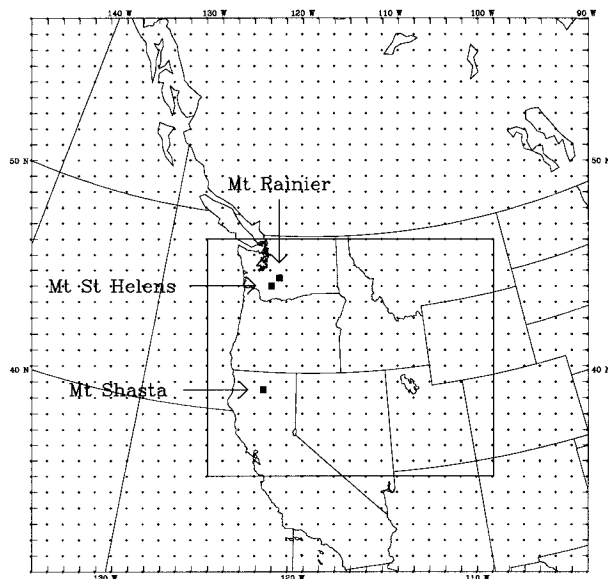
Climate Model Domain and Mountain Locations

FIG. 5. Climate model domain at 90-km resolution. Subgrid orographic precipitation and surface cover schemes are applied to the area within the rectangle. Also shown are the locations of three mountains described in the sensitivity experiments.

To provide a more physically based approach that alleviates this problem, we do not permit the ice to be any thinner than 0.1 m. If the ice mass per unit area is less than the product of the ice material density and the minimum ice thickness, then the ice is assumed to occupy only a fraction of the water body, with the ice fractional area given by the ratio of ice mass to the product of the ice material density and the minimum ice thickness. The ice thickness only exceeds the minimum ice thickness when the ice fractional area exceeds unity. Separate energy balances are used for the ice-free and ice-covered fractions of the lake.

3. Numerical experiments

The RCM is applied to the western United States where complex surface topograhy and diverse vegetation are the dominant geographical features. The model domain is depicted in Fig. 5, which shows the 90-km grid cells and the rectangular boundaries within which subgrid parameterizations have been applied. The model was driven by initial and lateral boundary conditions interpolated from the meteorological analysis by the European Centre for Medium-Range Weather Forcasts (ECMWF). Sea surface temperature was obtained from
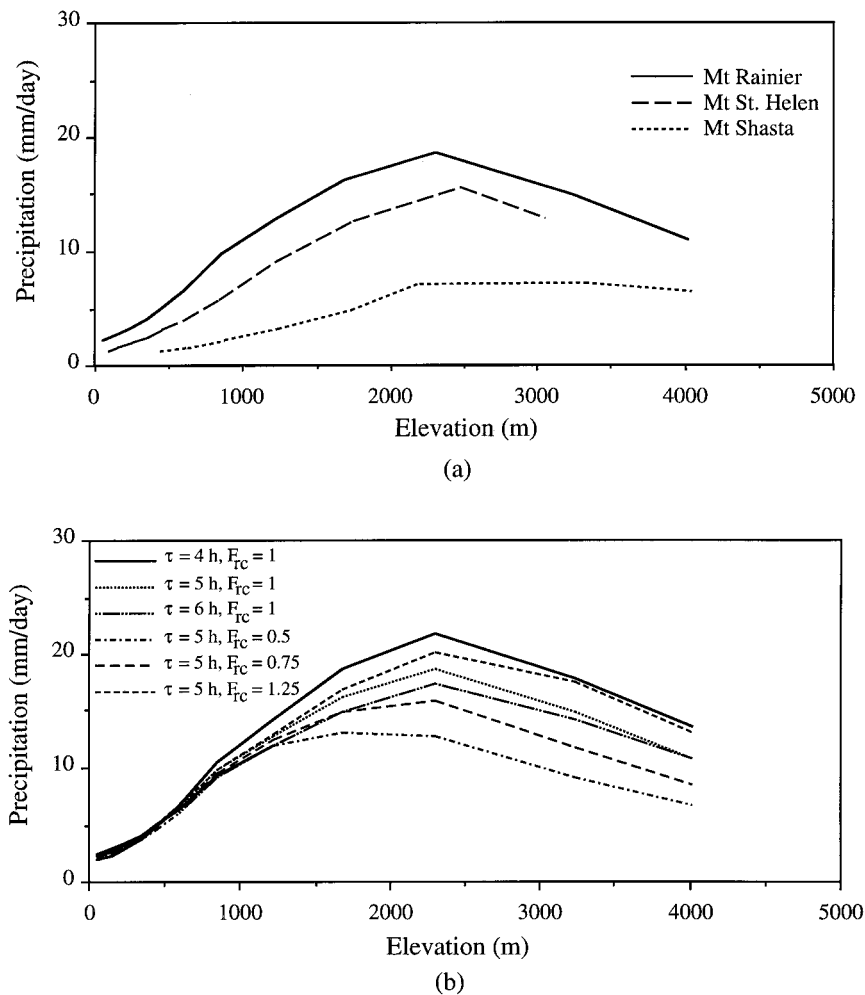
FIG. 6. Altitude–precipitation relationships simulated by the subgrid orographic precipitation scheme (a) at three mountain locations, and (b) at Mt. Rainier using different model parameters.

the NAVY 12-hourly gridded analysis. The simulation began on 1 October 1991; after the model spinup, sensitivity experiments were each performed for December 1991. We chose mainly the winter season to evaluate the subgrid parameterizations because the climatology in the Pacific Northwest shows a distinct precipitation maximum in winter. For evaluating the subgrid vegetation scheme, simulations were performed over summer as well. Finally, a long simulation that spans water years 1992–94 has been performed to evaluate the model performance in simulating precipitation and other surface climate over relatively wet, normal, and dry conditions.

We will focus on the surface hydrology of the Pacific Northwest. The simulated surface variables are mapped from elevation bands to geographical locations based on high-resolution surface elevation data and compared with observations according to the locations of the observing stations. We have examined different ways to perform the mapping; they will be discussed in the fol-

lowing section. Regional means will be calculated based on simple averaging of all the observations or simulations within regions that are defined by state boundaries. We will compare the simulated precipitation and surface temperature with observations at weather stations.

4. Test of subgrid orographic precipitation scheme

The subgrid parameterization of orographic precipitation was designed to be a computationally efficient method for representing the effects of topography on cloud processes in regional or global climate models. Leung and Ghan (1995) described the tuning of the orographic timescale, τ, and compared a 2-month-long wintertime simulation with observations in the Pacific Northwest. Here, we perform more testing of the parameterization by examining the effects of more parameters, and explore different methods for mapping the simulation at elevation bands to geographical locations and their impacts on the results.
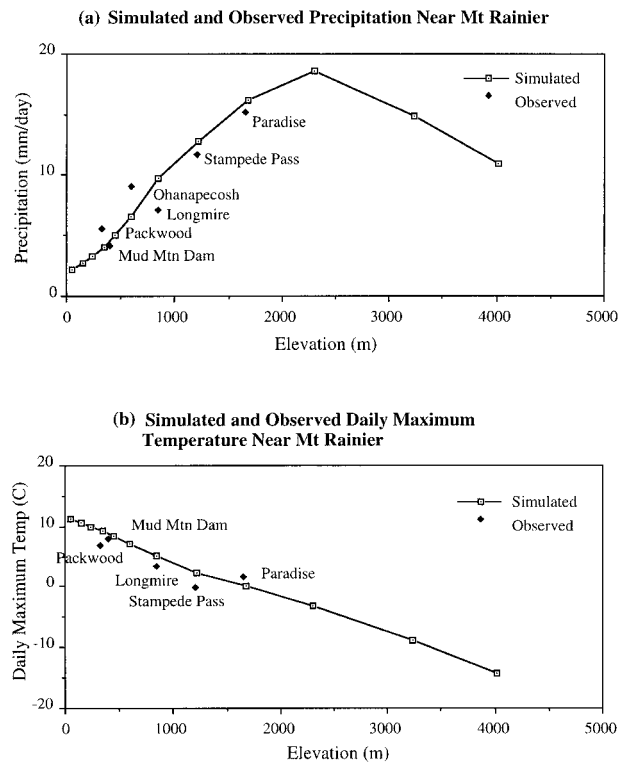
(a) Simulated and Observed Precipitation Near Mt Rainier

(b) Simulated and Observed Daily Maximum Temperature Near Mt Rainier

FIG. 7. Simulated and observed monthly mean (a) precipitation and (b) daily maximum surface temperature near Mt. Rainier.

a. Tuning of parameters

The strength of the orographic signal in precipitation depends on many factors such as the height and width of the mountain barrier and the flow characteristics and the moisture content of the air mass. To examine these factors, we plotted in Fig. 6a the relationships between altitude and precipitation simulated by the model at the three mountain locations indicated in Fig. 5. These locations are chosen because there is a wide range of surface elevation within the grid cells covering the mountains. Precipitation was averaged over the month of December 1991. Each point on the curves corresponds to the mean altitude of the elevation band versus the simulated precipitation within the model grid cell containing the mountain structures.

In general, precipitation increases as elevation increases up to a certain altitude, beyond which precipitaton decreases with elevation. A maximum in precipitation arises because as condensation is enhanced by orographic uplift, the available moisture content decreases (e.g, Burns 1953; Alpert 1986). Over Mt. St. Helens and Mt. Rainier, the altitude for maximum precipitation is around 2400 m; at Mt. Shasta, this altitude is much higher, around 3300 m, and precipitation decreases only slightly above this altitude. The similarity between simulations over Mt. St. Helens and Mt. Rainer is clearly because these mountains are located very close to one another; the air mass arriving there should have

very similar moisture content. Mt. Shasta is located much farther south and closer to the ocean; the incoming air mass contains more moisture over a deeper atmospheric column so that the altitude for maximum precipitation is higher up.

In our subgrid parameterization, τ and Fr_c are the only two tuning parameters that can affect the simulated orographic precipitation signature. Figure 6b shows a variety of altitude-precipitation relationships simulated at Mt. Rainier using different values of τ and Fr_c. In general, orographic signature increases as τ decreases and Fr_c increases, and it depends more strongly on the latter parameter, which determines the flow regime of air mass flowing over mountain barriers. Consistent with the analysis of Leung and Ghan (1995) for the whole Pacific Northwest rather than a specific location, the analysis here also shows the best agreement with observation at the local scale is obtained when τ is about 5 h, and Fr_c is approximately equal to unity. This set of parameters again yields the best agreement with observations when comparing both regional mean and correlation coefficient between observations and simulations over the whole Pacific Northwest region. It should also be noted that although the simulated precipitation is quite sensitive to τ and Fr_c at high altitude, it varies little with those parameters below 1000 m. Since most surface stations are located at the lower elevation, extensive evaluation of the parameterization scheme is difficult. On the other hand, areas with altitude much higher than the grid cell average usually occupy a very small fraction of the total area; problems introduced by sen-

TABLE 4. Sensitivity of model evaluation to postprocessing procedures.

Postprocessing method	Observed mean (mm day^{-1})	Simulated mean (mm day^{-1})	Precip. Corr.	Elevation corr.
Standard	3.84	3.44	0.56	0.98
1.5 km smoothed	3.84	4.07	0.54	0.88
3 km smoothed	3.84	4.14	0.58	0.88
6 km smoothed	3.84	4.31	0.59	0.84
9 km smoothed	3.84	4.50	0.58	0.85
18 km smoothed	3.84	4.57	0.57	0.75

TABLE 5. Observed and simulated daily maximum surface temperature in °C.

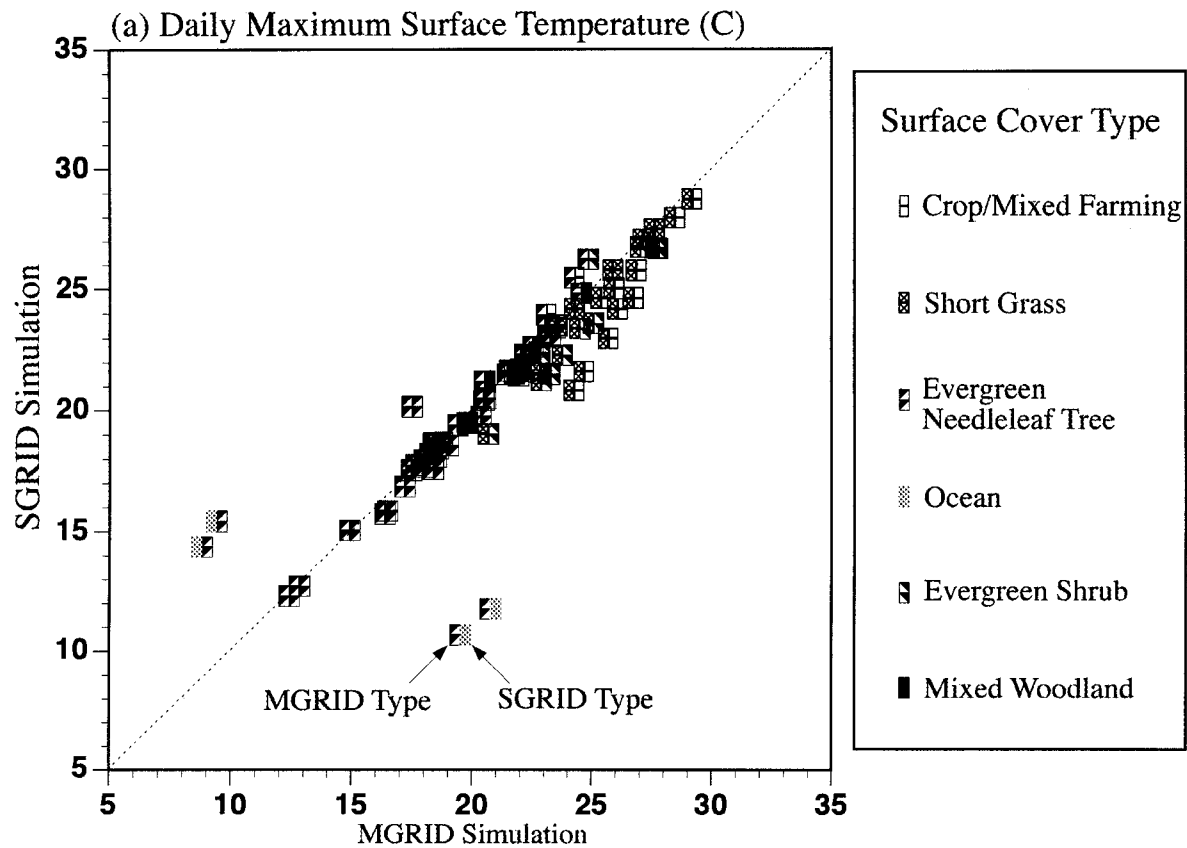| Month	Observed	MGRID simulation	SGRID simulation
Oct	16.6	19.2	18.4
Nov	8.2	10.9	9.5
Dec	6.1	9.1	8.7
Jan	6.4	9.2	8.5
Feb	9.8	12.2	11.5
Mar	15.1	16.4	15.7
Apr	16.5	17.4	16.7
May	22.6	24.5	23.6
Jun	25.9	27.4	26.5
Jul	25.8	28.1	27.1

FIG. 8. Scatterplots comparing the daily (a) maximum surface temperature, (b) sensible heat flux, and (c) latent heat flux simulated by the model with MGRID and SGRID surface cover.

sitivity of the simulation to model parameters are likely insignificant.

Unfortunately, observations in remote mountainous areas are very limited and are typically made at lower elevations. In Fig. 7, we can only show observations made at several stations on or near Mt. Rainier; all the stations, except Stampede Pass, are located within the same grid cell over Mt. Rainier. The simulated precipitation and surface temperature both agree quite well with observations. There is some variability (e.g., over Longmire and Ohanapecosh) that cannot be explained simply by elevation.

b. Sensitivity to postprocessing procedures

The subgrid parameterization predicts precipitation for each elevation band of each grid cell. We have developed postprocessing procedures to map the prediction back to a geographical map when comparing the simulation with observations. The standard method locates the four model grid cells surrounding a surface station, and for each grid cell, precipitation is interpolated from the prediction at the two elevation bands bracketing the altitude of the surface station. Predictions at the grid cells are bilinearly interpolated to station

locations. A correlation coefficient of 0.98 is obtained between the altitude of surface stations and the elevation interpolated at the locations of surface stations using the same procedure described above for precipitation over Washington State.

Since model evaluation may be dependent on the postprocessing method, we have examined other procedures to perform the mapping from elevation bands to geographical sites. Based on the 1.5-km elevation dataset used to produce the elevation classification scheme, smoothed elevation datasets are generated at different spatial resolutions by using moving averages for the mapping discussed above. The orographic precipitation signature is therefore inherently smoothed by such procedures.

Table 4 shows the regional mean of the observed and simulated precipitation in Washington State and the correlation coefficient obtained with the standard mapping procedure and the new procedure at different spatial resolutions. The last column shows the correlation coefficient between the station elevation and the elevation mapped to the station locations by the postprocessing methods. Since the model prediction is interpolated from the class mean elevation to the station elevation in the standard method, the correlation coefficient be-
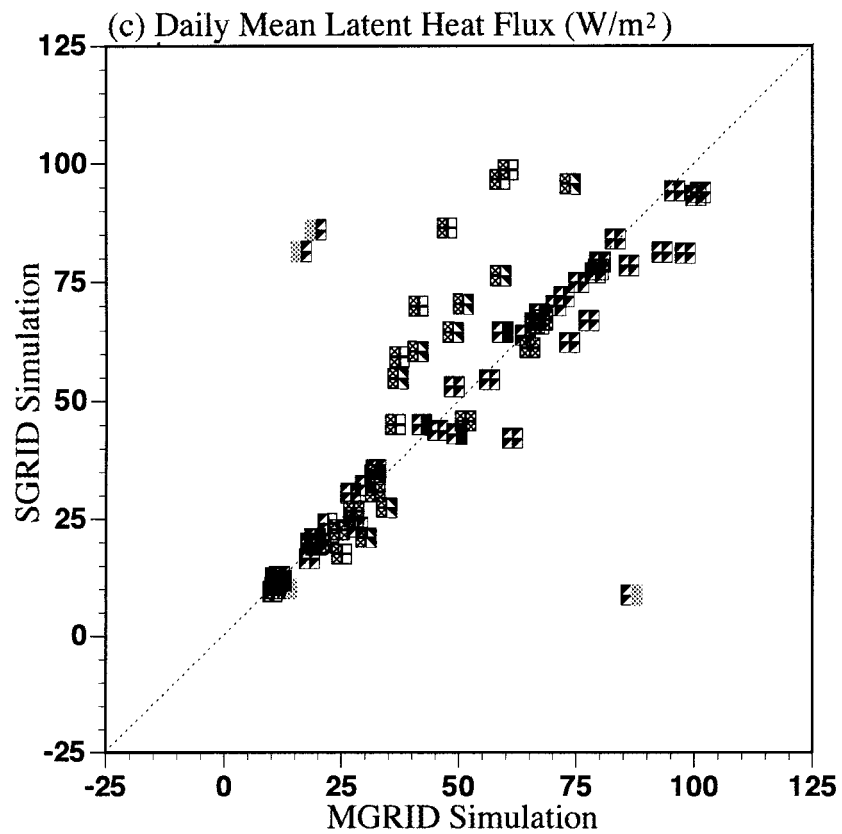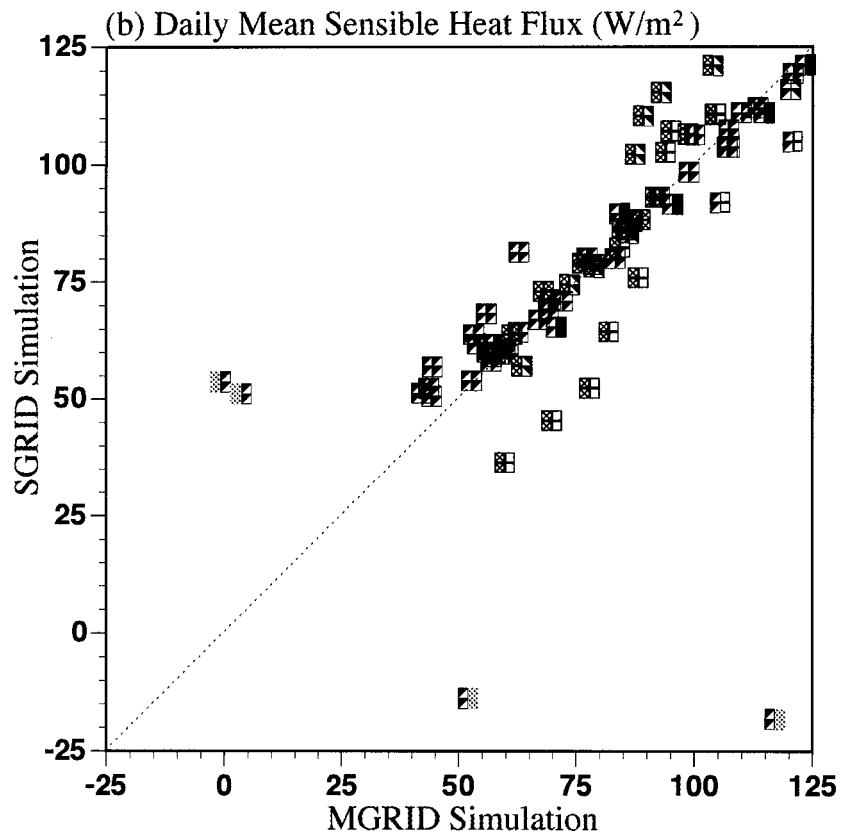
(b) Daily Mean Sensible Heat Flux (W/m²)

(c) Daily Mean Latent Heat Flux (W/m²)

FIG. 8. (*Continued*)

tween the station and mapped elevation is highest. However, the correlation coefficient between the observed and mapped precipitation simulation is relatively low compared with the new postprocessing procedure. With the new method, higher correlation is found when the spatial resolution is around 6 km. At the highest resolution (1.5 km), the correlation is actually the lowest. The largest difference among the correlation coefficients (between 0.59 and 0.54) is statistically significant at the 0.1 level. The other correlation coefficients are hence not significantly different from one another statistically. The different mapping procedures or resolutions also affect the regional mean precipitation of the simulation, with the latter increasing with coarser resolution. When mapping is performed at coarser resolution, the surface elevation corresponding to surface stations at the lower elevation would effectively be increased and hence higher precipitation would be mapped to those areas. The reverse is true for surface stations that are located at high elevation. Because more stations are located in low lying areas or valleys, the mean precipitation is increased as the mapping resolution is decreased.

This analysis shows that the orographic precipitation signature may be manifested more at coarser resolution such as 6 km; precipitation variations at the higher resolution (such as 1.5 km) do not necessarily relate to topographic features. Daly et al. (1994) also discussed the difficulty of defining an ''optimal'' spatial resolution for applying a statistical-topographic model (PRISM) to estimate the climatological precipitation patterns in mountainous areas. They found that the PRISM model performs better at 6-km resolution or coarser. This is partly related to the spatial scale of the data used, and the fact that some variability of precipitation is not related to topography or slope/aspect. Our analysis presented here is also limited by the spatial density of observations used.

5. Test of subgrid vegetation scheme

To examine the effects of the subgrid vegetation scheme on model simulation, we have performed two simulations, each beginning 1 October 1991 and ending 31 July 1992. One simulation (MGRID) was performed using the vegetation data derived from the 30-min global dataset (Fig. 2b) without subgrid representation, and the second simulation (SGRID) was performed with the subgrid vegetation scheme using data derived from AVHRR pixels. We focus our discussion on analysis of the simulation over Washington State because more dramatic differences are seen in the vegetation covers used by the two simulations.

Table 5 shows the monthly mean time series of daily maximum surface temperature from observations, the MGRID, and SGRID simulations averaged over Washington State. With the subgrid vegetation scheme, the regional mean surface temperature simulated by the model is generally about 1°C cooler than the MGRID

simulation, although there are warm biases in both simulations. No noticeable differences can be found between the MGRID and SGRID simulations of precipitation. The scatterplot shown in Fig. 8a compares the surface temperature of the two simulations at the locations of surface stations for June 1992. Different patterns are used to indicate the surface cover type used in the two simulations. The cooling in the SGRID simulation arises mainly because of a change in surface cover from short grass to farmland in the Columbia River basin. Figures 8b and 8c compare the sensible heat and latent heat flux from the two simulations. When farmland is used to describe the surface cover in the SGRID simulation instead of short grass in the MGRID simulation, the Bowen ratio is much lower, reflecting the stronger capability of farmland to transpire and reduce heat. Another major difference is found in the scatterplots showing areas assigned ocean versus land. This can be explained by Fig. 2a, which shows that when the subgrid vegetation scheme is used, the coastline can be represented with much finer detail.

The cooling simulated with the subgrid vegetation scheme helps reduce the warm bias found in previous simulations reported by Leung and Ghan (1995), in which the model was set up as the MGRID simulation. It should be emphasized that much of the change in surface cover used in the subgrid scheme has resulted from the use of the AVHRR data over the 30-min global vegetation data. The subgrid vegetation scheme further captures the subgrid heterogeneity that could be related to surface topography. The effects of the subgrid vegetation scheme alone (i.e., if MGRID is performed with grid cell mean vegetation derived from AVHRR data) are likely very small as can be deduced from the change in percent area listed in Table 2. On the other hand, when only one surface cover type is prescribed for each elevation band, no additional computation is associated with the use of the subgrid vegetation scheme.

6. Evaluation of lake simulation

There are precious few alpine lakes with multiyear research quality thermodynamic data. Of the lakes listed in Table 3, only two are measured enough to evaluate the lake model. Thus, we focus our evaluation on Pyramid and Yellowstone lakes.

Figure 9 compares simulated and observed surface temperature for the period October 1992–September 1994. The period prior to October 1992 is not shown because the simulation is highly affected by initialization, and inappropriate values for turbidity were used. The lake model simulates the annual cycle of surface temperature for Pyramid Lake fairly well, with wintertime errors of less than 2°C and summertime errors of 2°–3°C. The timing of the annual cycle is correct, but the amplitude is 10%–20% too weak. Measurements at Yellowstone are only available during the summer months when it is not frozen; data are missing in 1994.
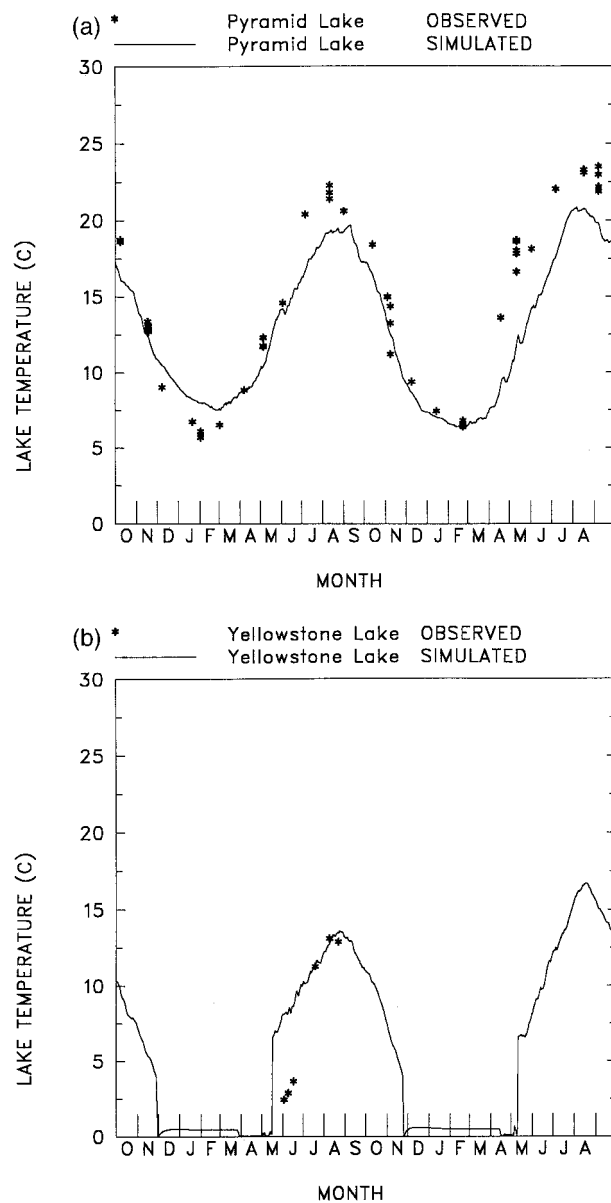
FIG. 9. Observed (asterisk) and simulated (solid line) lake surface temperature at (a) Pyramid and (b) Yellowstone Lakes for the period October 1992–September 1994.
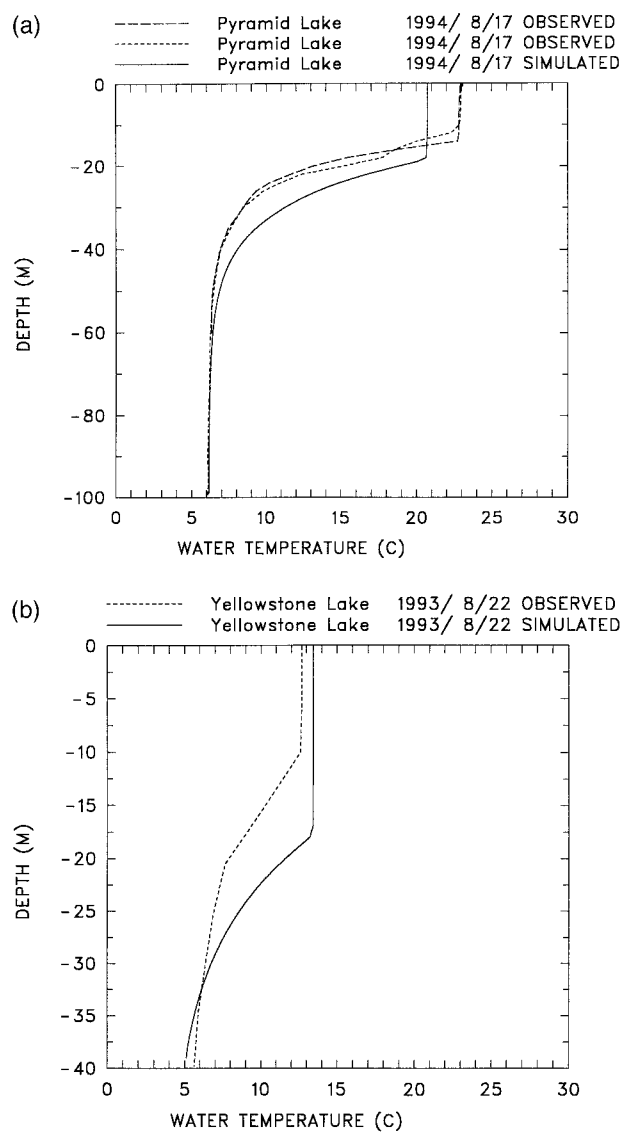

FIG. 10. Observed (dashed line) and simulated (solid line) lake temperature profiles at (a) Pyramid Lake over two locations for 17 August 1994 and at (b) Yellowstone Lake for 22 August 1993.

The lake model correctly simulates the maximum surface temperature in August, but appears to warm the lake too soon in June.

The vertical profile of the simulated lake temperature is evaluated in Fig. 10. During the winter months the lakes are generally isothermal. During the summer months a thermocline develops as a result of absorption of sunlight and stirring by surface winds. The lake model simulates the development of a thermocline of approximately the correct depth. The deep lake temperatures are in excellent agreement with the measurements. However, the reader should note that these results are

quite sensitive to the value of the turbidity, which varies not only from lake to lake but is also known to vary from month to month.

The ice mass loading simulated for Yellowstone Lake is illustrated in Fig. 11. Although observations of ice thickness are not available, general freezing and melting dates of Yellowstone Lake are known (A. Siebecker 1997, personal communication). Lake freezing usually occurs in late December, about one month later than simulated. Ice melting is usually completed in late May or early June, a week or two later than simulated. It is not clear why the simulated lake ice melts sooner than observed. The early freezing is likely due to the excessively cold (about 5°C) surface temperature simulated for Yellowstone Lake. The cold bias at Yellowstone
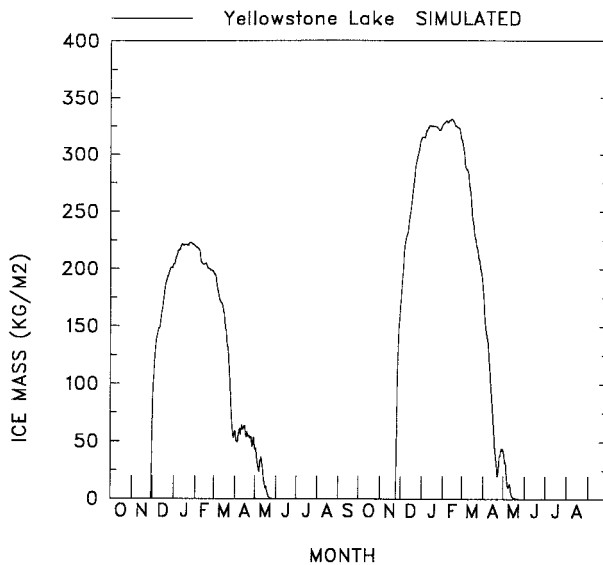
FIG. 11. Simulated ice mass loading at Yellowstone Lake for the period October 1992–September 1994.

FIG. 12. Scatterplot comparing the observed and simulated precipitation averaged over all winter months for each station in Washington State.

Lake is due to the higher surface elevation of the elevation class that represents the lake; a more refined representation of elevation classes would reduce this bias and the associated early freezing of the lake.

7. Evaluation of a 3-yr climate simulation

With the subgrid parameterizations all tested, a 3-yr simulation has been performed with the PNNL-RCM for water years 1992–94. This period represents 3 yr with relatively dry, wet, and normal climate conditions. The El Niño conditions during the winter of 1992 result in warmer temperature and less precipitation in the Pacific Northwest (e.g., Cayan and Webb 1992). The simulation is performed using $\tau = 5$ h and $Fr_c = 1$. The standard postprocessing method described in section 4b is used to map the model prediction from elevation classes to geographic locations for model evaluation.

Figure 12 shows the observed and simulated precipitation over each station in Washington State. As seen in Fig. 1, Washington State represents a region with a very high degree of variation in surface elevation. Both the observation and simulation shown are averages over December and January of all simulation years. The correlation coefficient is around 0.7, and the mean observed and simulated precipitation are 4.21 and 3.94 mm day^{-1}, respectively. As discussed by Leung and Ghan (1995), the use of the subgrid orographic precipitation scheme mainly improves the simulation of precipitation over regions of complex terrain and during wintertime. When the subgrid scheme is used, the distribution of precipitation is altered to reflect the effects of surface elevation on cloud and precipitation processes, and hence leads to improvement in the simulation. In summer, the correlation coefficient between observed and simulated pre-
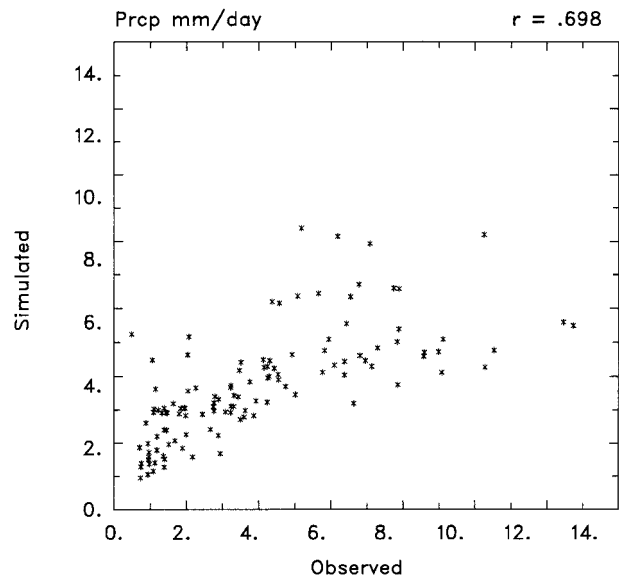
cipitation remains low, around 0.2 to 0.4. The same remains true in the multiyear simulation reported here.

Figure 13 shows time series of observed and simulated regional mean for surface temperature and precipitation. As expected when the model was driven by global analysis, the simulation follows closely the interannual variability of the observed conditions. The model also correctly simulated the wintertime maximum in precipitation in the maritime regime (Washington and Oregon) and the summertime maximum in precipitation in the continental area (Idaho and Montana). There is, however, a general small dry bias in the model simulation. Since most weather stations are located at the lower elevation, this dry bias reflects the tendency of the subgrid parameterization to overreduce precipitation at low elevation. In the subgrid parameterization, orographic uplift is accounted for by an airflow model. The airflow model does not parameterize downslope flow; the thermodynamic model simply assumes adiabatic descent when air parcels move down valley. Hence there is a tendency for the model to dry and warm the lower elevation bands. Since this tendency is dependent on the orographic timescale τ, one way to model the lower elevation more realistically is to use a longer timescale for the descending airflow down valleys. In the future, we will experiment with more physically based methods to model the downslope flow in the subgrid parameterization.

Surface temperature is simulated relatively well over Washington and Oregon. However, a warm bias (2°–4°C) is found over Idaho and Montana and the problem is more serious in summer. One reason for the warm bias has already been described above as related to the treatment of downslope flow in the subgrid scheme.

Warming is induced through adiabatic descent of air parcels as well as reduction of cloud cover. The latter can cause a more serious problem in summer. Furthermore, the airflow factor tends to induce a larger warm bias over Idaho and Montana because the averaged station elevation is lower than the area-averaged surface elevation by a greater margin in those two regions than in Washington and Oregon. To determine if other factors are responsible for the warm bias, we tested the use of smaller diffusivity for vertical mixing as recently implemented in MM5 Version 2. This change affects only the stable nightime turbulence regime. The daily minimum surface temperature was reduced by $1°–3°C$ during winter as a result of the change. However, the effect is much less during summer. Hence it is more likely that the summer warm bias is also related to the radiation and surface parameterizations.

8. Summary and discussion

Surface topography explains a high percentage of spatial variability in precipitation over mountainous regions. The prediction of orographic precipitation has important implications for the prediction of surface hydrology such as snow cover and streamflow. An efficient way of modeling orographic precipitation is through subgrid parameterization. An example of such schemes has been developed by Leung and Ghan (1995). Here we have described further evaluation of the subgrid parameterization of orographic precipitation as implemented in a regional climate model. To complement the model evaluation performed by Leung and Ghan, who compared model simulation with observations at the regional scale, this paper focuses on evaluating the subgrid parameterization at the subgrid scale to determine whether the relationships between precipitation and surface elevation can be simulated in mountainous areas within grid cells. Also, a longer simulation has been performed to determine if the year-to-year variability can be captured by the model. This study suggests that the parameters used in the subgrid orographic scheme are quite robust; the same set of parameters that was found to be optimal in Leung and Ghan (1995) also applies when evaluation is performed at the subgrid scale, and over a multiyear period.

Based on the parameterization, cloud, radiation, boundary layer, and surface processes are all modeled explicitly over each elevation class of a model grid cell. This method is found to perform quite well in the Pacific Northwest. Wintertime precipitation simulated at the local and regional scales has been compared with observations. In the model simulation, precipitation typically increases to a maximum at the crest of the topographic barrier over lower mountains. This is consistent with studies over mountain barriers in the midlatitudes (e.g., Barry 1973; Hanson et al. 1980). However, the model-simulated relationships between surface elevation and precipitation showed an altitude for maximum precip-

itation below the crest of some high mountains. This height varies according to the flow characteristics and moisture content of air masses.

We have also examined the aggregation of surface cover by elevation classification. Although the subgrid vegetation scheme is implemented such that multiple vegetation covers can be described within each elevation band of each grid cell, for computational efficiency we only defined each elevation band by a dominant surface cover and sizable lakes. Clearly, not all the subgrid variability in surface cover can be explained by surface elevation. One obvious reason is that human activities such as farming have altered the surface cover significantly in the Pacific Northwest. Another factor is related to the vegetation classification used by BATS. The distinction between evergreen needle and mixed tree, or short versus tall grass, is probably more detail than can be explained by simple elevation dependence. Nevertheless, by using a high-resolution vegetation dataset and the subgrid representation of surface cover, the surface cover represented in the model is significantly different from that which was derived from a 30-min global dataset without the subgrid scheme. The effect on the model simulation is a slight regional cooling of about $1°C$, which helps to reduce the warm bias found in the model simulation.

A lake model has been implemented in the regional climate model to simulate the thermodynamics of lakes that are either explicitly resolved by the model grid cells, or represented by the subgrid surface cover scheme. The lake model performs as well for the alpine lakes as it does for the Great Lakes (Bates et al. 1995). Biases in ice formation have been traced to the coarse vertical resolution of the subgrid surface elevation scheme.

Our modeling approach has been to develop a basic framework such that more physically based parameterizations and sophisticated subgrid representations of surface characteristics can be incorporated in climate models progressively, evaluating the improvements added to the simulations at each step. We have identified several areas where it can be further developed. On the subgrid orographic precipitation scheme, we found that model bias can arise from the simple treatment of downslope flow, which tends to dry and warm the subgrid lower elevations. Studies on flow over complex terrain suggested that air being drained to valleys sometimes follows adiabatic descent from hill tops. However, quite frequently, air temperature over valleys is not very different from that over hill tops, implying an isothermal temperature profile. Stability is one factor causing the thermal structures in valleys to differ or resemble those of the higher elevations. Also needed to be considered is nocturnal drainage flow, which introduces nightime cooling along valleys. In the future, we will develop a more physically based method for modeling downslope flow.

Another area worth investigating is the effects of orography on convective precipitation. Is our subgrid
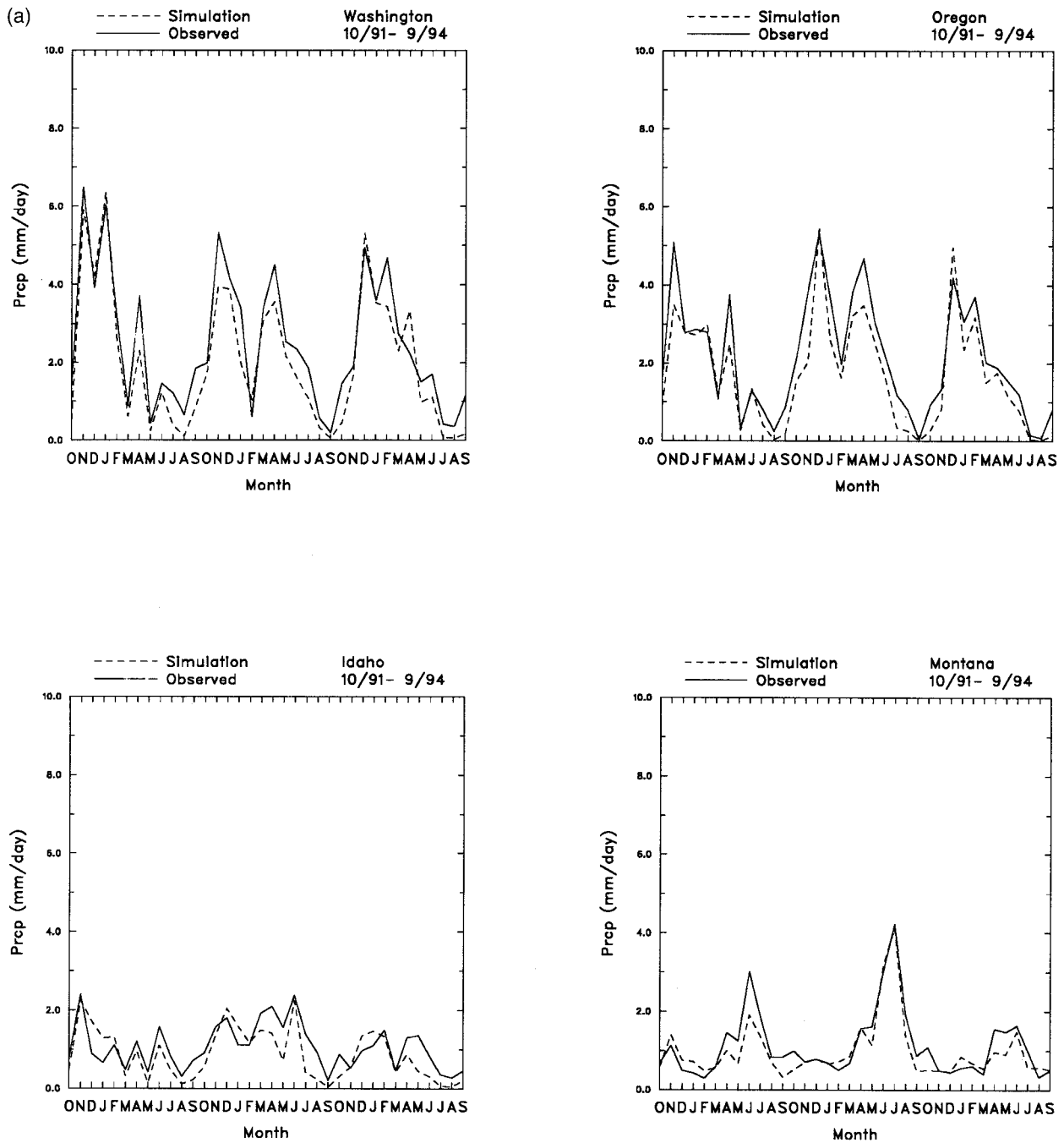
FIG. 13. Time series of simulated and observed regional mean (a) precipitation, and (b) daily maximum surface temperature.

parameterization able to model the redistribution of convective precipitation over complex topography? Clearly, by modifying the vertical profiles of θ_c and r_w [Eqs. (5) and (6)] through the airflow model, the subgrid parameterization affects the atmospheric stability, which is often used in cumulus parameterization schemes for triggering convective adjustment. Furthermore, the amount of convective precipitation can differ among

elevation classes simply because of the different amount of moisture available. Leung and Ghan (1995) compared summertime simulations of precipitation in the Pacific Northwest at 90-km resolution with and without the subgrid orographic precipitation scheme. They found that when the subgrid scheme is used, a small improvement is found in the simulation when compared with observations. In future studies, we will examine in more
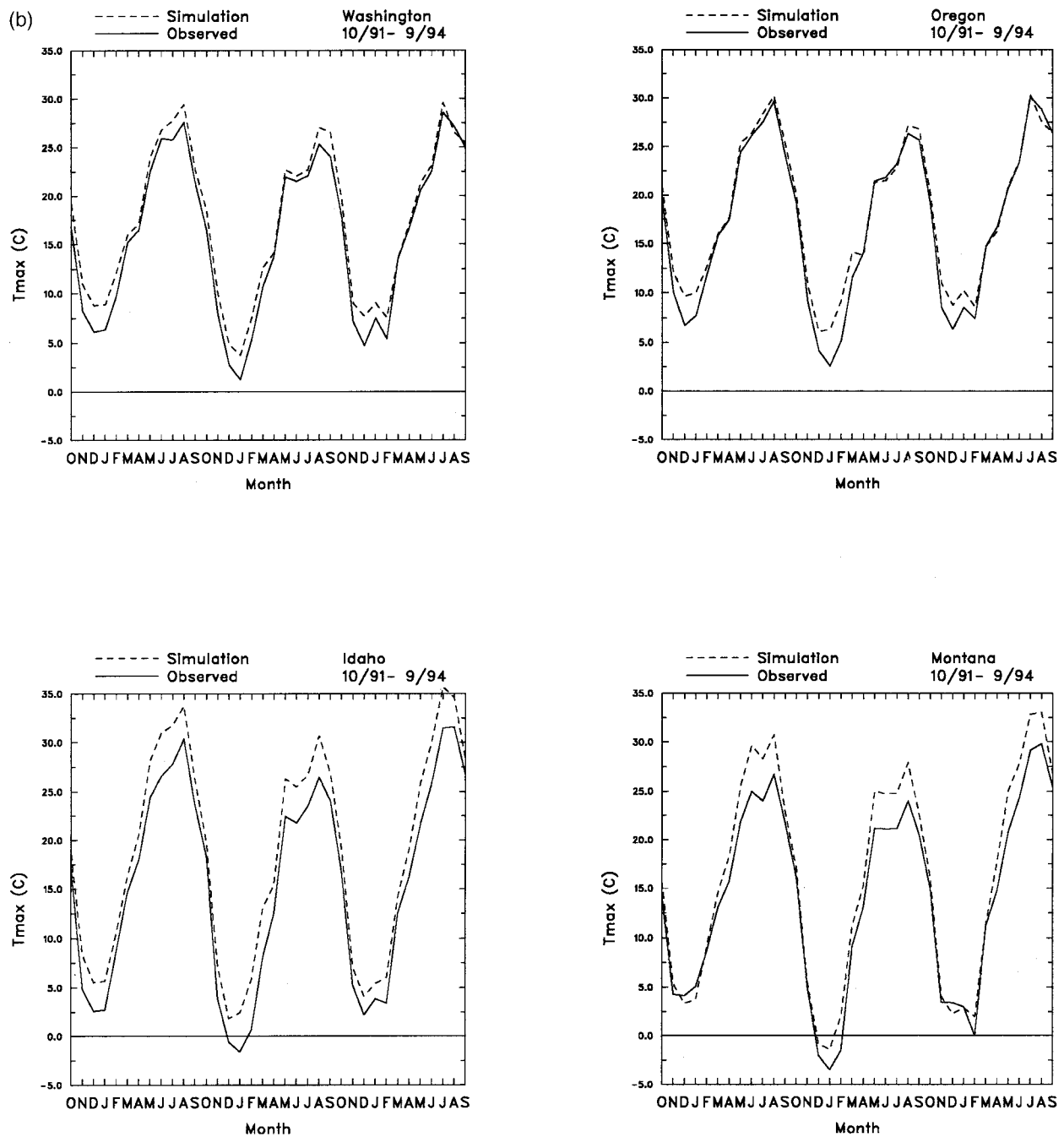
(b)

FIG. 13. (*Continued*)

detail the ability of the subgrid parameterization to correctly simulate the orographic effects on convective precipitation.

Finally, the subgrid surface scheme can be easily extended to account for the subgrid variability of other surface characteristics. For example, soil properties such as texture, depth, and albedo can exert a strong influence on surface processes, even dominating over the effects of heterogeneous vegetation under some atmospheric

and surface conditions. By using the State Soil Geographic Data Base, which is a comprehensive soil database developed for the United States, we can aggregate the soil information again by surface elevation within each model grid cell. In this way, the interactions between soil, vegetation, and the atmosphere can be represented with higher spatial detail in climate models. We will also evaluate our subgrid parameterizations over other geographic locations. High-resolution (about

1 km) Digital Elevation Model data have now become available over most regions of the world. Our surface elevation classification scheme can be modified to efficiently represent subgrid variations in surface elevation in other areas, and the subgrid orographic precipitation scheme can then be applied and evaluated globally. Subgrid parameterizations accounting for variability of precipitation due to orography, vegetation, and soil are excellent alternatives to a mesoscale modeling technique that uses model nesting to explicitly resolve precipitation at the grid scale. Because the use of subgrid parameterizations requires much less computational time, long-term simulation is feasible, and useful climate information can be provided at the subgrid scale, which is most needed for assessing climate change and its impacts on hydrology and vegetation.

REFERENCES

Alpert, P., 1986: Mesoscale indexing of the distribution of orographic precipitation over high mountains. *J. Climate Appl. Meteor.,* **25,** 532–545.

Anthes, R. A., E. Y. Hsie, and Y. H. Kuo, 1987: Description of the Penn State/NCAR Mesoscale Model Version 4 (MM4). NCAR Tech. Note NCAR/TN-282+STR, National Center for Atmospheric Research, Boulder, CO, 66 pp. [Available from NCAR, P.O. Box 3000, Boulder, CO 80307.]

Avissar, R., 1992: Conceptual aspects of a statistical-dynamical approach to respresent landscape subgrid-scale heterogeneities in atmospheric models. *J. Geophys. Res.,* **97,** 2729–2742.

——, and R. A. Pielke, 1989: A parameterization of heterogeneous land surfaces for atmospheric numerical models and its impacts on regional meteorology. *Mon. Wea. Rev.,* **117,** 2113–2136.

——, and F. Chen, 1993: Development and analysis of prognostic equations for mesoscale kinetic energy and mesoscale (subgrid scale) fluxes for large-scale atmospheric models. *J. Atmos. Sci.,* **50,** 3751–3774.

Barbour, M. G., J. H. Burk, and W. D. Pitts, 1987: *Terrestrial Plant Ecology.* Benjamin/Cummings, 634 pp.

Barry, R. G., 1973: A climatological transect on the east slope of the Colorado Front Range. *Arct. Alp. Res.,* **5,** 89–110.

Bates, G. T., S. W. Hostetler, and F. Giorgi, 1995: Two-year simulation of the Great Lakes region with a coupled modeling system. *Mon. Wea. Rev,* **123,** 1505–1522.

Betts, A. K., 1973: Non-precipitation cumulus convection and its parameterization. *Quart. J. Roy. Meteor. Soc.,* **99,** 178–196.

Burns, J. I., 1953: Small-scale topographic effects on precipitation distribution in San Dimas experimental forest. *Trans. Amer. Geophys. Union,* **34,** 761–768.

Cayan, D. R., and R. H. Webb, 1992: El Niño/Southern Oscillation and streamflow in the western United States. *El Nino: Historical and Paleoclimatic Aspects of the Southern Oscillation,* H. F. Diaz and V. Markgraf, Eds., Cambridge University Press, 29–88.

Cotton, W. R., G. J. Tripoli, R. M. Rauber, and E. A. Mulvihill, 1986: Numerical simulation of the effects of varying ice crystal nucleation rates and aggregation processes on orographic snowfall. *J. Climate Appl. Meteor.,* **25,** 1658–1680.

Daly, C., R. P. Neilson, and D. L. Phillips, 1994: A statistical–topographic model for mapping climatological precipitation over mountainous terrain. *J. Appl. Meteor.,* **33,** 140–158.

Dickinson, R. E., A. Henderson-Sellers, and P. J. Kennedy, 1993: Biosphere–Atmosphere Transfer Scheme (BATS) Version 1e as coupled to the NCAR Community Climate Model. NCAR Tech. Note NCAR/TN-387+STR, National Center for Atmospheric Research, Boulder, CO, 72 pp. [Available from NCAR, P.O. Box 3000, Boulder, CO 80307.]

Entekhabi, D., and P. Eagleson, 1989: Land surface hydrology parameterization for atmospheric general circulation models including subgrid scale spatial variability. *J. Climate,* **2,** 816–831.

Ghan, S. J., and R. C. Easter, 1992: Computationally efficient approximations to stratiform cloud parameterization. *Mon. Wea. Rev.,* **120,** 1572–1582.

Grell, G., 1993: Prognostic evaluation of assumptions used by cumulus parameterizations. *Mon. Wea. Rev.,* **121,** 764–787.

——, J. Dudhia, and D. R. Stauffer, 1993: A description of the fifth-generation Penn State/NCAR Mesoscale Model (MM5). NCAR Tech. Note NCAR/TN-398+IA, National Center for Atmospheric Research, Boulder, CO, 107 pp. [Available from NCAR, P.O. Box 3000, Boulder, CO 80307.]

Guo, Y.-R., and S. Chen, 1993: Terrain and land use for the fifth-generation Penn State/NCAR mesoscale modeling system (MM5). NCAR Tech. Note NCAR/TN-397+IA, National Center for Atmospheric Research, Boulder, CO, 113 pp. [Available from NCAR, P.O. Box 3000, Boulder, CO 80307.]

Hanson, C. L., R. P. Morris, R. L. Engleman, D. L. Coon, and C. W. Johnson, 1980: Spatial and seasonal precipitation distribution in southwest Idaho. Agricultural reviews and manuals, ARMW-13, U.S. Department of Agriculture, Science and Education Administration, 15 pp. [Available online at http://www.access.gpo.gov.]

Hostetler, S., and P. J. Bartlein, 1990: Simulation of lake evaporation with application to modeling lake level variations in Harney-Malheur Lake, Oregon. *Water Resour. Res.,* **26,** 2603–2612.

——, G. T. Bates, and F. Giorgi, 1993: Interactive coupling of a lake thermal model with a regional climate model. *J. Geophys. Res.,* **98,** 5045–5057.

International GEWEX Project Office, 1994: Implementation plan for the GEWEX Continental-scale International Project (GCIP), Vol II, Research. International GEWEX Project Office, Washington, DC, 120 pp. [Available from International GEWEX Project, 1100 Wayne Ave., Suite 1210, Silver Spring, MD 20910.]

Kiehl, J. T., R. J. Wolski, B. P. Briegleb, and V. Ramanathan, 1987: Documentation of radiation and cloud routines in the NCAR Community Climate Model (CCM1). NCAR Tech. Note NCAR/TN-288+IA, National Center for Atmospheric Research, Boulder, CO, 105 pp. [Available from NCAR, P.O. Box 3000, Boulder, CO 80307.]

Koster, R. D., and M. J. Suarez, 1992: Modeling the land surface boundary in climate models as a composite of independent vegetation stands. *J. Geophys. Res.,* **97,** 2697–2717.

Leung, L. R., and S. J. Ghan, 1995: A subgrid parameterization of orographic precipitation. *Theor. Appl. Climatol.,* **52,** 95–118.

——, M. S. Wigmosta, S. J. Ghan, D. J. Epstein, and L. W. Vail, 1996: Application of a subgrid orographic precipitation/surface hydrology scheme to a mountain watershed. *J. Geophys. Res.,* **101,** 12 803–12 817.

Lott, F., and M. J. Miller, 1997: A new subgrid-scale orographic drag

parameterization: Its formulation and testing. *Quart. J. Roy. Meteor. Soc.,* **123,** 101–128.

Loveland, T. R., J. W. Merchant, D. O. Ohlen, and J. F. Brown, 1991: Development of a land-cover characteristics database for the conterminous U.S. *Photogramm. Eng. Remote Sens.,* **57,** 1453–1463.

Patterson, J. C., and P. F. Hamblin, 1988: Thermal equilibrium of a lake with winter ice cover. *Limnol. Oceanogr.,* **33,** 323–338.

Pielke, R. A., G. A. Dalu, J. S. Snook, T. J. Lee, and T. G. F. Kittel, 1991: Nonlinear influence of mesoscale land use on weather and climate. *J. Climate,* **4,** 1053–1069.

Raupach, M. R., 1993: The averaging of surface flux densities in heterogeneous landscape. Exchange processes at the land surface for a range of space and time scales. *Proc. Yokohoma Symp.,* Yokohoma, Japan, International Association Hydrol. Sci., 343–355.

Sheppard, P. S., 1956: Airflow over mountains. *Quart. J. Roy. Meteor. Soc.,* **82,** 528–529.

Shuttleworth, J., 1996: GCIP coupled modeling workshop. IGPO publication series 23, International GEWEX Project Office, Silver Spring, MD, 20 pp. [Available from International GEWEX Project Office, 110 Wayne Ave., Suite 1210, Silver Spring, MD 20910.]

Smith, R. B., 1980: Linear theory of stratified hydrostatic flow past an isolated mountain. *Tellus,* **32,** 348–364.

——, 1989: Mountain induced stagnation points in hydrostatic flows. *Tellus,* **41A,** 270–274.

Taylor, K. E., and S. J. Ghan, 1992: An analysis of cloud liquid water feedback and global climate sensitivity in a general circulation model. *J. Climate,* **5,** 907–919.

Vankat, J. L., 1982: A gradient perspective on the vegetation of Sequoia National Park, California. *Madrono,* **29,** 214–220.

Whittaker, R. H., 1956: Vegetation of the Great Smokey Mountains. *Ecol. Monogr.,* No. 26, Ecol. Soc. Amer., 1–80.

Zeng, X., and R. A. Pielke, 1994: A generalized boundary layer theory over inhomogeneous terrain. Preprints, *Sixth Conf. on Mesoscale Processes,* Portland, OR, Amer. Meteor. Soc., J32–J35

Zhang, D. L., and R. A. Anthes, 1982: A high-resolution model of the planetary boundary layer—Sensitivity tests and comparisons with SESAME-79 data. *J. Appl. Meteor.,* **21,** 1594–1609.

Zhong, S., and J. C. Doran, 1995: A modeling study of the effects of inhomogeneous surface fluxes on boundary layer properties. *J. Atmos. Sci.,* **52,** 3129–3142.

——, and ——, 1997: A study of the effects of spatially varying fluxes on cloud formation and boundary layer properties using data from the Southern Great Plains Cloud and Radiation Testbed. *J. Climate,* **10,** 327–341.